ELSEVIER

Integrating tracer experiments with modeling to assess runoff processes and water transit times

K.J. McGuire [a,*], M. Weiler [b], J.J. McDonnell [c]

[a] *Center for the Environment, Plymouth State University and USDA Forest Service, Northeastern Research Station, Plymouth, NH 03264, USA*
[b] *Departments of Forest Resources Management and Geography, University of British Columbia, Vancouver, BC, Canada V6T 1Z4*
[c] *Department of Forest Engineering, Oregon State University, Corvallis, OR 97331, USA*

Abstract

Representing runoff process complexity in a simple model structure remains a challenge in hydrology. We present an integrated approach to investigate runoff processes using a hillslope tracer experiment and modeling exercise to explore model parameterization, process representation, and transit times. A spatially-explicit model constrained by soil hydrologic properties, runoff, and applied tracer data was used to identify the dominant processes necessary to explain both water and solute flux from a steep hillslope. The tracer data allowed for the rejection of model parameter sets based on the calibration to runoff data alone, thus reducing model uncertainty. The additional calibration to tracer data, improved parameter identifiability and provided further insight to process controls on hillslope-scale water and solute flux. Transit time distributions developed using the model provided further insight to model structure such as sub-surface volume, mixing assumptions, and the water table dynamics. Combining field experiments with the modeling exercise may lead to a more comprehensive assessment of runoff process representation in models.
© 2006 Elsevier Ltd. All rights reserved.

Keywords: Modeling; Multi-criteria calibration; Transit time; Hillslope hydrology; Tracer application

1. Introduction

Field studies in hillslope hydrology often reveal complex hydrological processes that operate across a range of spatial and temporal scales and antecedent wetness conditions [1,9,18]. These complex hydrological descriptions that we develop from field studies are difficult to incorporate within a modeling framework due to the disparity between the scale of measurements and the scale of model sub-units and the natural heterogeneity of catchments [6,8]. Thus, many hydrologists have moved away from fully distributed physically-based models and toward more conceptually-based models that describe dominant hydrological processes at the hillslope and catchment

scales [4,8]. However, parameters represented in many conceptual models are often not physically-based or related to physical properties, and therefore cannot be established prior to a model calibration-validation exercise. An additional problem is that the information content in a rainfall-runoff record limits the complexity of conceptual model structures available to test and explore internal process dynamics [27,31,51].

Recent model calibration approaches have constrained parameterizations using additional data sources such as tracers [68], groundwater levels and estimated saturation areas [20,21], and other multiple measures [22,42]. Multi-criteria calibration approaches often result in less adequate, but acceptable fits to observed runoff data (compared to calibration using runoff alone) that are generally more consistent with process findings [51]. These models, which focus on internal process dynamics and less on calibration-based schemes, are necessary in reducing predictive

---

* Corresponding author. Tel.: +1 603 535 3250; fax: +1 603 535 3180.
E-mail address: kmcguire1@plymouth.edu (K.J. McGuire).

uncertainty and to develop new model descriptions that match the level of process understanding and available data information content [56]. This is particularly important as interest in catchment water quality increases [13,15,38], since water sources, stores, and pathways within hillslopes and catchments must be adequately represented in models to predict and understand the behavior of solutes (e.g., geochemistry, contaminants, or conservative tracers). Catchment modelers are increasingly challenged to incorporate water quality aspects into models to deal with problems such as acidification [61], cumulative effects [53], nutrient cycling [16], total maximum daily loads, and contamination. The age or transit time of water offers a link to water quality since the contact time in the subsurface largely controls stream chemical composition, revealing information about the storage, flow pathways and source of water in a single measure.

The transit time distribution represents the integrated hillslope or catchment scale response of the diverse flow pathways that participate in solute transport, thus connecting process complexity with model simplification. Water transit times are typically determined by black-box modeling of environmental tracers (e.g., ^{18}O, ^{2}H, ^{3}H, CFCs, and SF_6), in which input (rainfall) and output (discharge) tracer concentrations are used to estimate parameters of an assumed time-invariant distribution that represents the transit time [36,39,67]. With this approach, however, we are unable to directly characterize the shape of the transit time distribution (TTD) and examine the assumption of time-invariance, which are undoubtedly important in controlling the fate and transport of solutes at the hillslope and catchment scales under natural rainfall conditions. While there has been some recent work on deriving transit time distributions from a theoretical perspective based on stochastic-mechanistic models [33,54], there has been little experimental work to directly determine the distribution of transit times with the exceptions of Nyström [45] and Rodhe et al. [49] (from roof-covered catchment studies), especially during non-steady-state conditions.

Monitoring applied tracers through storm and non-storm periods offers an alternative approach to black-box modeling, where tracer breakthrough curves can be measured to infer transit time distributions in a more experimental fashion rather than the inverse estimation problem of parameterizing simple black-box models. There have been numerous applied tracer studies on hillslopes [10,12,26,34,44,46,66]; however, most of these studies did not focus on determining hillslope-scale transit time distributions and interpretative models were largely solute transport models (i.e., convection-dispersion models) as opposed to coupled hydrologic-tracer models.

The coupling of solute tracer and hydrologic models allows for a comprehensive evaluation of model structure, in terms of predicting runoff and tracer, and verification that the model is working for the right reasons and is consistent with our understanding of reality [30,70]. There are very few catchment models that incorporate tracers in a spatially-explicit manner with limited complexity. For example, HSPF, a commonly used and highly parameterized hydrologic simulation model that is coupled with water quality models, is difficult to calibrate due to the number of parameters and their non-uniqueness [17]. There is a critical need to simplify process complexity to achieve parsimonious models that transcend scaling issues and represent dominant physical processes [55].

In this study, we combine the merits of an applied tracer experiment at the hillslope scale and a simple, spatially-explicit hydrologic model to: (1) identify the dominant processes necessary to explain both water and solute flux, (2) test a simple, parsimonious model constrained by soil hydrologic, runoff, and applied tracer data, and (3) use the model as an exploratory tool to directly infer potential hillslope transit time distributions under steady and non-steady conditions. Our work builds upon the study of Weiler and McDonnell [71] that introduced a model for performing "virtual experiments" at the hillslope-scale for the purposes of exploring first-order controls on hydrological processes in a controlled environment. Here we apply the same model to a field tracer experiment in an effort to simplify observed process complexity and then use the model to investigate dominant process controls on water transit time.

2. Site description

The study was conducted in Watershed-10 (WS10, 10.2 ha), which is part of a larger research effort at the H.J. Andrews Experimental Forest (HJA) Long-Term Ecological Research (LTER) program in the west-central Cascade Mountains of Oregon, USA (44.2°N, 122.25°W) (Fig. 1). WS10 has a temperate maritime climate with wet mild winters and cool dry summers. The mean annual precipitation is 2220 mm (averaged from 1990 to 2002), about 80% of which falls between October and April during long duration, low to moderate intensity frontal storms. Relatively light snow accumulations are common, but seldom persist longer than 1–2 weeks and generally melt within 1–2 days. No significant snow accumulation was observed during this study (9 December 2002 to 31 March 2003). On average, 56% (range: 28–76%) of the annual precipitation becomes runoff. The vegetation is dominated by a naturally regenerated second growth Douglas-fir (*Pseudotsuga menziesii*) stand resulting from a 1975 clear-cut harvest.

The hillslope study area is located on the south aspect of WS10, 91 m upstream from the stream gauging station (Fig. 1). The 125 m long stream-to-ridge slope is slightly convex with an average gradient of 37°, ranging from 27° near the ridge to 48° adjacent to the stream. Elevation ranges from 480 to 565 m. The hillslope is underlain by bedrock of volcanic origin, including andesitic and dacitic tuff and coarse breccia [62]. Soils, formed either
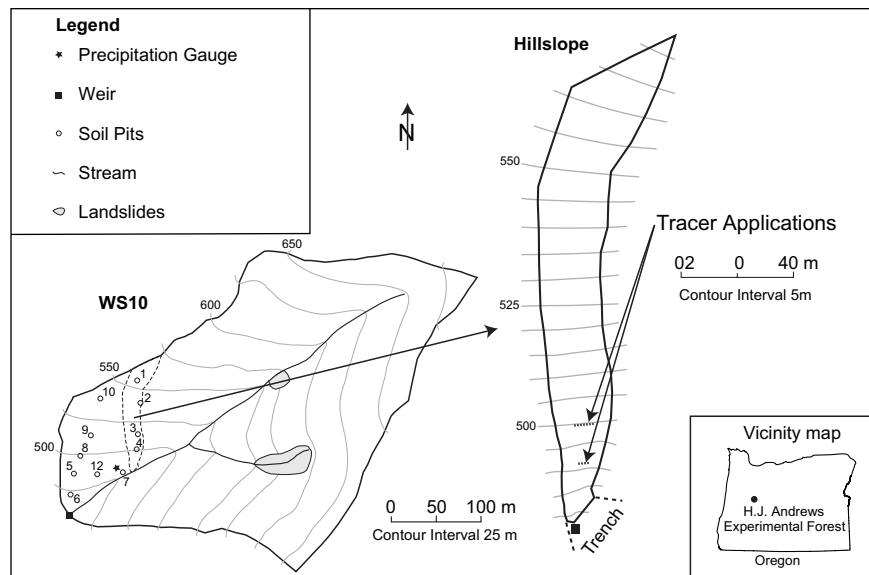
Fig. 1. Map of the study area.

in residual parent material or in colluvium originating from these deposits, are classified as Typic Dystrochrepts [69,59]. Soil textures range from gravelly, silty clay loam to very gravelly clay loam. Surface soils are well aggregated, but lower depths (70–110 cm) exhibit more massive blocky structure with less aggregation than surface soils [24,59]. Beneath the weakly developed A and B horizons is relatively low permeability, partially weathered parent material (saprolite) ranging in thickness from 1 to 7 m [48,59]. The depth to unweathered bedrock ranges from 0.4 to 0.6 m at the stream–hillslope interface and increases gradually toward the ridge to approximately 3–8 m. Harr and Ranken [25,59] had excavated eleven soil pits on the study slope (Fig. 1) and collected at least six undisturbed soil cores from each pit at depths of 10, 30, 70, 110, 130, and 150 cm (200 and 250 cm cores were collected where feasible), totaling 452 soil cores. The soil cores were analyzed for hydrologic properties including hydraulic conductivity, porosity, pore-size distribution, moisture characteristics, and stone content [24,48]. Mean values of the six replicated cores were reported in archived data records (Forest Service Data Bank, maintained by the HJA LTER program).

Relatively well defined seeps have been identified flowing from the base of the hillslope soils into the stream channel [24,63]. These seeps are highly localized zones of saturated soil related to the microtopography of the unweathered bedrock near the stream or to the presence of vertical, andesitic dikes approximately 5 m wide, which are located within the southern aspect hillslope [24,62]. Maximum water table development over the bedrock surface on this hillslope never exceeded 25 cm in thickness. The main rationale for selecting this study slope was the richness of local data resources from these previous studies [24,48,58,59,63].

3. Field methods and results

3.1. Field methods

A 10 m long trench was constructed to measure subsurface flow at a natural seepage face using steel sheeting that was driven approximately 5 cm into the exposed bedrock and then sealed with hydraulic cement to intercept subsurface water. Intercepted subsurface water was routed to a calibrated 15° V-notch weir that recorded stage at 10-min time intervals using a 1-mm resolution capacitance water-level recorder (TruTrack, Inc., model WT-HR). Precipitation was measured with a tipping bucket and storage gauge in a small canopy opening on the hillslope. A roof was constructed over the trench to prevent interception of direct precipitation and no surface overland flow was observed during the study. The drainage area of the hillslope was delineated topographically from a total station survey (130 points) of the entire hillslope (0.17 ha) and verified by a water balance calculation. We used a rounded value of 0.2 ha in all analyses. A detailed knocking pole survey [76] of the lower 30 m of hillslope was used to determine bedrock topography (Van Verseveld, unpublished data) and extend soil depth data collected by Harr and Ranken [25].

Two line source tracers were applied to the hillslope immediately before a large winter rainstorm (66 mm, 49.5 h duration) that began on 9 December 2002 at 21:30 h. 20.9 g of Amino G acid monopotassium salt (AGA), a fluorescent dye [57], and 4.0 kg of bromide (as LiBr solution) were applied 19 and 33 m (slope distance) from the trench, respectively. AGA is preferred over other fluorescent dyes since it has lower adsorptive loss in soils [64]. The AGA was injected using syringes beneath the organic horizon soil over a 2.5 m long application line

and Br⁻ was sprayed onto the soil surface with a backpack sprayer along a 5.0×0.10 m application area. The AGA concentrations were measured at 2-min intervals for 9 days using a field fluorometer equipped with a flow-through cell, data logger, and long wavelength optical kit (Turner Designs, Inc., Sunnyvale, CA, model 10-AU). Bromide was also measured *in situ* using an ion-selective electrode (TempHion®, Instrumentation Northwest, Inc., accuracy = ±5%) and recorded on a Campbell CR10X (Campbell Scientific, Inc.) data logger at 5-min time intervals until 31 March 2003. Grab samples were collected from the start of the experiment until 18 February 2003 at both the trench (AGA: 272 samples, Br: 107 samples) and at the WS10 catchment outlet (AGA: 257 samples, Br: 270 samples). The AGA grab samples were analyzed in the laboratory using the same fluorometer, whereas Br⁻ samples were filtered and analyzed using an ion chromatograph at the Boise Aquatic Sciences Lab (Rocky Mountain Research Station, Boise, ID). Background apparent concentrations of AGA were evaluated at the hillslope during a storm prior to the tracer experiment. Maximum background AGA concentrations, which coincided with discharge peaks, ranged from 3 to 10 μg L⁻¹. Background Br⁻ concentrations were not detectable (<0.45 mg L⁻¹).

3.2. Field results: tracer breakthrough

The response to the tracer application was extremely rapid (Fig. 2). Tracer concentrations peaked 40.4 and 40.3 h (61.2 mm of rainfall) after the start of the storm (9 December 2002 21:30 h), for AGA and Br⁻, respec-

tively. These response times indicate that subsurface flow velocities were 0.47 and 0.82 m h⁻¹ for the AGA and Br⁻, respectively, based on the rainfall initiation time. The near synchronous response of both tracers suggests strong lateral preferential flow and little difference in transport between the two application distances. During the first 10 days of the experiment, both AGA and Br⁻ concentrations were high and responsive to rainfall with somewhat smoother Br⁻ concentrations indicating higher dispersion compared to the AGA tracer (Fig. 2b, inset). After this period, the concentrations began to slowly recede and recovery rates decreased. Overall, 19% and 53% of the applied tracer mass was recovered for AGA and Br⁻ at the trench site, respectively. No detectable concentrations of either tracer were observed at the WS10 outlet, mainly due to dilution from the higher discharge in the stream (~2 orders of magnitude volumetric flow). We expected higher recovery rates of AGA, since it was applied much closer to the hillslope trench; however, the low AGA recovery was likely an artifact of sorption to organic material. Also, due to difficulties in quantifying background concentrations (see [57]), the AGA recovery is uncertain and likely overestimated. Hence, we did not model the AGA breakthrough data.

4. Modeling methods and results

4.1. Modeling methods

We used a simple physically-based hillslope model, Hill-Vi, to describe water and solute flux at our hillslope under
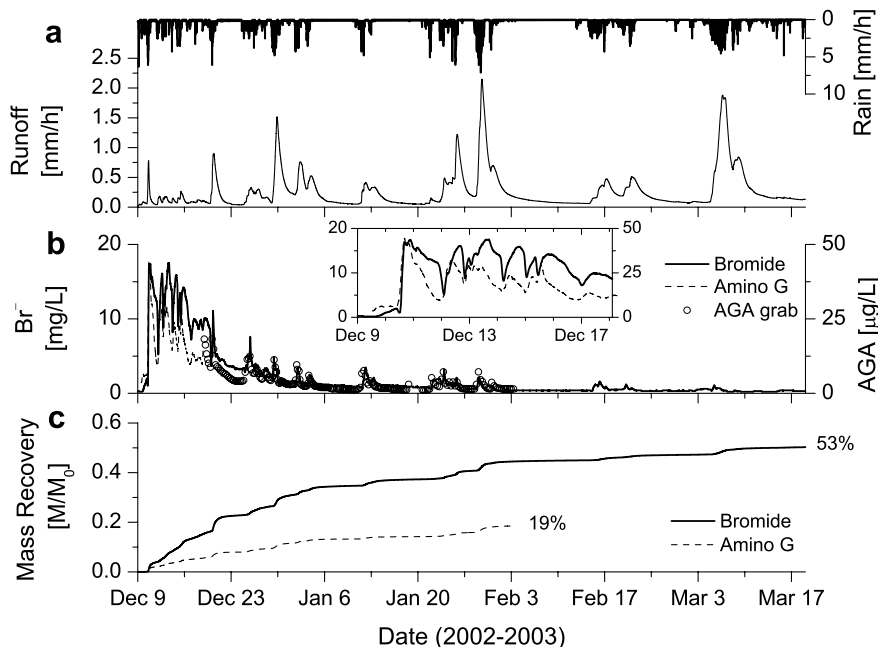

Fig. 2. Time series of observed rainfall and runoff (a), breakthrough of bromide and Amino G acid (AGA) (b), and tracer mass recovery (M/M_0 is cumulative mass relative to injected mass) (c). Bromide and AGA were sampled continuously from 9 December 2002; however, beginning on 19 December, grab samples were collected at 4–7 h intervals for AGA until 4 February 2003 when concentrations were at or below background levels. The first 9 days of breakthrough (b) are expanded in the inset figure and the beginning of the x-axis indicates the start of the experiment (9 December 2002 21:30).

natural rainfall conditions during the tracer experiment. This model was introduced by Weiler and McDonnell [71] as a tool to perform virtual experiments on hillslopes to address process controls on the generation of subsurface flow. Hill-Vi has been used in subsequent work to test nutrient flushing hypotheses [73] and to explore the effects of pre-event water variability on estimated runoff components and the connectivity of hillslope preferential flow networks [74]. This is the first study to use Hill-Vi in conjunction with a field experiment. We based the model structure on our best process understanding determined from WS10 past field investigations [24,25,48]. We present only a brief overview of the model here, highlighting specific features that relate to runoff generation in WS10. Detailed descriptions of the overall model are provided by Weiler and McDonnell [71,73].

Hill-Vi is a spatially explicit model that solves basic continuity equations within coupled unsaturated and saturated zones. The unsaturated-saturated zone coupling was implemented to represent unsaturated zone conversion to transient saturation during storm events, which is observed frequently in field studies [2,24,37,41]. The unsaturated zone is defined by the depth from the soil surface to the water table and is characterized by time-variable water content [52]. The saturated zone is defined over an impermeable or semi-impermeable bedrock surface by the thickness of the water table and the porosity, n. Lateral subsurface flow is calculated using the Dupuit–Forchheimer assumption and routed downslope using the approach of Wigmosta and Lettenmaier [75], according to the water table gradients between grid cells. Lateral subsurface flow only occurs within the saturated zone.

Hill-Vi uses a depth function for drainable porosity as a control on transient water table development [71]. The drainable porosity is defined by the difference in volumetric water content between 0 and 100 cm of water potential (i.e., approximately from saturation to field capacity). Field observations show that the drainable porosity declines dramatically with depth due to changes in the soil structure and macropore development. Fig. 3a shows the drainable porosity calculated from soil core data collected at WS10 and an exponential function and prediction limits (95%) that indicate the overall trend and variability in drainable porosity with depth. The drainable porosity, n_d, is represented in the model by the following function:

$$n_{\mathrm{d}}(z) = n_0 \exp\left(-\frac{z}{b}\right), \tag{1}$$

where n_0 is the drainable porosity at the soil surface and b is a decay coefficient.

We calculate the water balance of the unsaturated zone by the rainfall input, vertical recharge into the saturated zone, and change in water content. Recharge from the unsaturated zone to the saturated zone is controlled by a power law relation of relative saturation within the unsaturated zone and the saturated hydraulic conductivity (K_{sat}) at the depth of the water table, $z'(t)$:

$$R(t) = \left(\frac{\theta(t)}{\theta_s}\right)^c k_0 \exp\left(-\frac{z'(t)}{f}\right), \tag{2}$$

where R is recharge to the saturated zone, θ/θ_s describes the relative water content, c is the power coefficient reflecting a nonlinear response to increased wetness, z' describes the location of the water table surface, k_0 is the surface K_{sat}, and f is the hydraulic conductivity shape factor for an

a

$n_d = n_0\exp(\text{-}z/b)$
$n_0 = 0.26$
$b = 1.12$
$r^2 = 0.77$

b

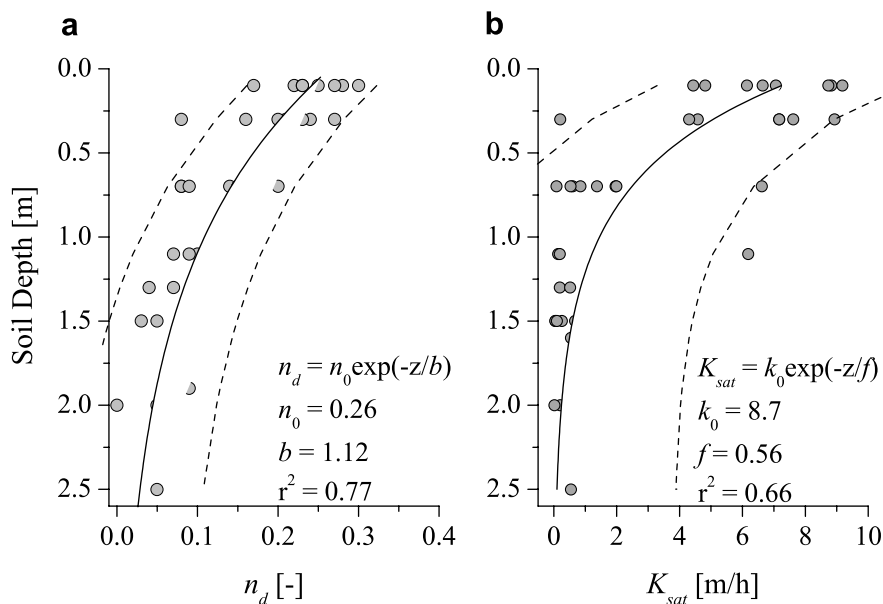$K_{sat} = k_0\exp(\text{-}z/f)$
$k_0 = 8.7$
$f = 0.56$
$r^2 = 0.66$

Fig. 3. Measured saturated hydraulic conductivity (K_{sat}) and drainable porosity (n_d) from soil pits shown in Fig. 1 [48] fit to exponential functions (solid line). Drainable porosity is taken as the difference in volumetric water content between saturation and 100 cm of tension. Each point represents the mean of six cores and the dashed lines are the 95% prediction limits.

exponential K_{sat} function. Fig. 3b shows the exponential reduction and considerable variability in K_{sat} determined from the WS10 data [48]. Eq. (2) represents the vertical water flux component described by Harr [24], which is essentially based on the Brooks and Corey [11] method. The water balance of the saturated zone in each grid cell is defined by the recharge input from the unsaturated zone, the lateral inflow and outflow, and the corresponding change of water table depth.

Actual evapotranspiration, E_{act}, is simply estimated based on the relative water content in the unsaturated zone (θ/θ_s) and the potential evapotranspiration, E_{pot} [5,51]:

$$E_{act}(t) = E_{pot}\left(\frac{\theta(t)}{\theta_s}\right). \tag{3}$$

Potential evapotranspiration was assumed a constant value in this study equal to the mean E_{pot} estimated with a temperature index model [23] (1 mm d^{-1}), since climatic and moisture conditions remain relatively constant through the winter period at the HJA. Rainfall interception loss was calculated using empirical relationships developed for the HJA [50], even though forest canopy characteristics were likely dissimilar. Keim et al. [29] showed that storm-to-storm variability in interception exceeds any differences in stand structure, age, and tree size; thus, we used Rothacher's [50] regression model develop for the HJA to provide a first-order approximation for any interception loss.

Solute flux in recharge, m_r, depends on the average concentration in the unsaturated zone and is determined by:

$$m_r(t) = R(t)\frac{M_{un}(t)}{S_{un}(t)n_{eff}}, \tag{4}$$

where $R(t)$ is the recharge of a grid cell at time t and S_{un} is the water storage in the unsaturated zone, and n_{eff} is the effective porosity (total porosity (n) × effective porosity coefficient ($^*n_{eff}$)). Effective porosity is a common simplification describing the porosity available for fluid flow and thus, the available pore space for solute mass transfer [3,60]. The lateral subsurface solute flux is calculated in a similar fashion by multiplying the subsurface flow with the average concentration in the saturated zone. Mass exchange between the saturated and unsaturated zone under transient water table conditions is contingent on the change in water table depth (Δw) and the difference between n_{eff} and n_d (i.e., the proportion of water that is drained by the falling water table). Weiler and McDonnell [71] showed that under a falling water table, solute is transferred (Δm) from the saturated to the unsaturated zone depending on the change in water table position, Δw, and the average concentration in the saturated zone:

$$\Delta m(t) = \frac{M_{sat}(t)}{w(t)n_{eff}}\Delta w(t)(n - \overline{n_d}), \tag{5}$$

$$\overline{n_d} = \frac{n_0 b}{\Delta w(t)}\left[\exp\left(-\frac{w(t)+\Delta w(t)}{b}\right) - \exp\left(-\frac{w(t)}{b}\right)\right], \tag{6}$$

where M_{sat} is the actual mass of solute in the saturated zone, $\overline{n_d}$ is average drainable porosity between the water table, $w(t)$, at time t and $\Delta w(t)$, which is the change in water table depth from the previous time step. If the water table is rising, the mass transfer depends on the average concentration in the unsaturated zone [71]:

$$\Delta m(t) = \frac{M_{unsat}(t)}{[D - w(t)]n_{eff}}\Delta w(t)(n - \overline{n_d}), \tag{7}$$

where D is the soil depth and M_{unsat} is the actual mass of solute in the unsaturated zone. We assume that the rising water table can only mobilize solute within the newly saturated portion of the soil profile. The concentrations in the saturated and unsaturated zone are calculated under the assumption of complete mixing in each zone and each grid cell.

We found during early model runs that too much tracer had been retained in the unsaturated zone, which was an artifact of our well-mixed unsaturated zone assumption. Thus, a bypass term was introduced that allowed for wetness dependent bypass of the unsaturated zone, a process that has been frequently observed in aggregated soils [47] and in other hillslope studies [14,32,37]. Bypass flow, q_{bp}, is dependent on the precipitation rate and soil moisture:

$$q_{bp}(t) = P\left(\frac{\theta(t)}{\theta_s}\right)^\beta, \tag{8}$$

where P is the precipitation rate and β is the bypass power coefficient. The mass flux of bypass flow is also assumed as the average concentration in the unsaturated zone similar to Eq. (4).

The model domain was established using a DEM (4×4 m) constructed from the topographic and soil depth survey, which extended beyond the delineated topographic drainage boundary. Measured soil hydrologic properties were used to parameterize the model; however, as illustrated by Fig. 3, there was large variability in the measured data values. Therefore, a Monte Carlo search was performed over expected parameter ranges based on the field data. The objective criteria used to assess model performance were the Nash–Sutcliffe efficiency (E) [43] for runoff and mass flux. Due to model computation time (30 minutes per model run), a detailed uncertainty analysis (e.g., [7]) was not performed; however, we include relative uncertainty measures and scattergrams of Monte Carlo parameter sets (1000 runs) and the Nash–Sutcliffe efficiencies. We defined uncertainty based on the top 20% performing parameter sets as the range between parameter values of the 0.1 and 0.9 percentiles divided by the median parameter value expressed as a percentage, consistent with the approach of Seibert and McDonnell [51]. Therefore, lower uncertainty values indicate a well-conditioned parameter value.

After a calibrated model was achieved (i.e., using field data and inverse methods), we assumed that it provides a first-order approximation for hillslope subsurface flow and transport, and is sufficient for performing numerical

experiments (i.e., scenarios) to examine hillslope-scale transit time distributions. Transit time, which describes the time for tracer to travel from entry to exit in the hillslope, can be directly simulated by applying a conservative tracer instantaneously to the entire hillslope:

$$TTD(t) = \frac{C_I(t)}{\int_0^\infty C_I(t)\,\mathrm{d}t} = C_I(t)Q(t)/M, \qquad (9)$$

where $TTD(t)$ is the transit time distribution from the model, $C_I(t)$ is the concentration of instantaneously applied tracer at $t = 0$ and M is the tracer mass applied to the entire surface of the hillslope in the model domain. Thus, the boundary conditions of our model differ from the field experiment so that tracer is distributed uniformly over the entire hillslope. Since many theoretical transit time distributions are derived for steady-state systems (e.g., [19,35]), we first simulated a steady-state case by running the model with a constant rainfall rate (i.e., average of the study period). Then, we simulated the dynamic case under natural rainfall conditions where we produced different TTD realizations by injecting tracer at monthly intervals from 1 November (immediately after driest three months) to 1 March (the middle of the wet season). All tracers were applied in the model on the first of the month and were simulated for one year (roughly the time of 100% mass recovery for this hillslope domain).

4.2. Modeling results: the line-source tracer experiment

Model calibration for the line-source tracer experiment was based equally on two criteria: (1) how well simulated runoff fit the observed hillslope runoff (runoff efficiency) and (2) how well the simulated mass flux fit observed bromide mass flux (mass flux efficiency). The best parameter set identified in the Monte Carlo analysis (i.e., the average of the two efficiency measures) was also the best parameter set based on only the mass flux E. The parameters for this model are shown in Table 1 along with the best parameter set based on the runoff E. The identifiability of the parameters is illustrated by the scattergrams in Figs. 4 and 5 and

by the relative uncertainty values listed in Table 1. Only a few of the parameters appeared to be identifiable (i.e., converge toward a maxima) based on the E criterion for runoff alone (n, b, c, and β) (Fig. 4). When the model was calibrated based on the mass flux E, several parameters resulted in different optimum values (n, f, k_0, and c). Even though, the efficiency was lower for mass flux, many of the parameters were more identifiable and had lower relative uncertainties (Fig. 5, Table 1). Also, the additional mass flux objective criterion, increased parameter identifiability from calibration determined based on only runoff for b, n_0, f, and k_0. Most calibrated values fell within the range obtained from measured soil hydrologic properties (Table 1). For instance, parameters defining the drainable porosity and K_{sat} depth functions were well within the range of the prediction limits shown in Fig. 2. The exceptions were the total porosity calibrated to the runoff data and shape factor, f, calibrated to the mass flux data.

Fig. 6 shows the model simulations and observed data time series. The best parameter set selected based on mass flux had efficiencies of 0.84 (runoff) and 0.59 (mass flux), while the best parameter set selected based on runoff had efficiencies of 0.92 (runoff) and 0.19 (mass flux) (Table 1). Although, both models produced reasonable simulations compared to runoff, our objective was to simulate both runoff and tracer. Using tracer mass flux as an additional objective criterion we were able reject the best runoff parameter set, since it fit the mass flux poorly (Fig. 6b, $E = 0.19$). Runoff efficiencies were between 0.76 and 0.88 for parameter sets that produced mass flux $E > 0.50$. Mass recovery for both models slightly deviate from the observed recovery; however, the best runoff parameter set significantly under-predicts mass flux during the first 2 weeks of the experiment, when about half of the total recovery occurred. The best mass flux parameter set recovered tracer similarly to the observations for the first 2 weeks when most of the tracer was exported. These recovery rates were based on the local mass recovery at hillslope grid cells that represented the trench face. Mass recovery for the entire model domain was 99% for

Table 1
Model parameter description, data limits, values used in simulations

Parameter	Description	Data		Model parameter sets	
		Lower limit	Upper limit	Model 1[a] (uncertainty[b])	Model 2[a,c] (uncertainty)
n	Average soil porosity	0.42	0.56	0.58 (25%)	0.41 (34%)
b (m)	Shape factor for drainable porosity function	1	2	1.61 (34%)	1.50 (34%)
n_0	Surface drainable porosity	0.17	0.30	0.20 (48%)	0.20 (36%)
f (m)	Shape factor for hydraulic conductivity function	0.5	0.8	0.66 (30%)	0.80 (13%)
k_0 (m h^{-1})	Surface hydraulic conductivity	4.4	9	8.84 (42%)	6.67 (25%)
c	Recharge power coefficient	23[d]	114[d]	75.2 (41%)	44.9 (71%)
β	Bypass power coefficient	–	–	13.5 (68%)	10.4 (80%)
*n_{eff}	Effective porosity coefficient	–	–	–	0.55 (46%)

[a] Best parameter sets determined by fit to runoff (model 1) and mass flux (model 2) observed data, respectively. Model 1 efficiencies were 0.92 and 0.19 and model 2 efficiencies were 0.84 and 0.59 for runoff and mass flux, respectively.
[b] Uncertainty is defined as range between the 0.1 and 0.9 percentile divided by the median for the top 20% performing (i.e. based on E) parameter values.
[c] Selected parameter set for transit time model scenarios.
[d] Estimated using the Brooks and Corey [11] pore-size distribution index.
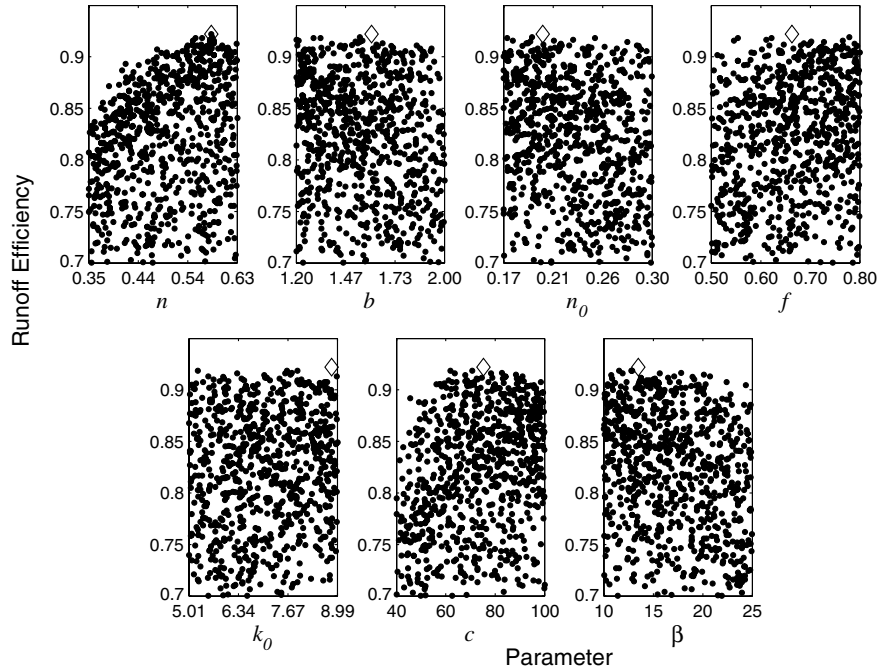
Fig. 4. A scattergram of 1000 Monte Carlo model simulations, where each point represents one model run with different randomly selected parameters within the range shown by the x-axes and its associated Nash–Sutcliffe efficiency [43] for runoff. The large diamonds indicates the best parameter set for runoff.
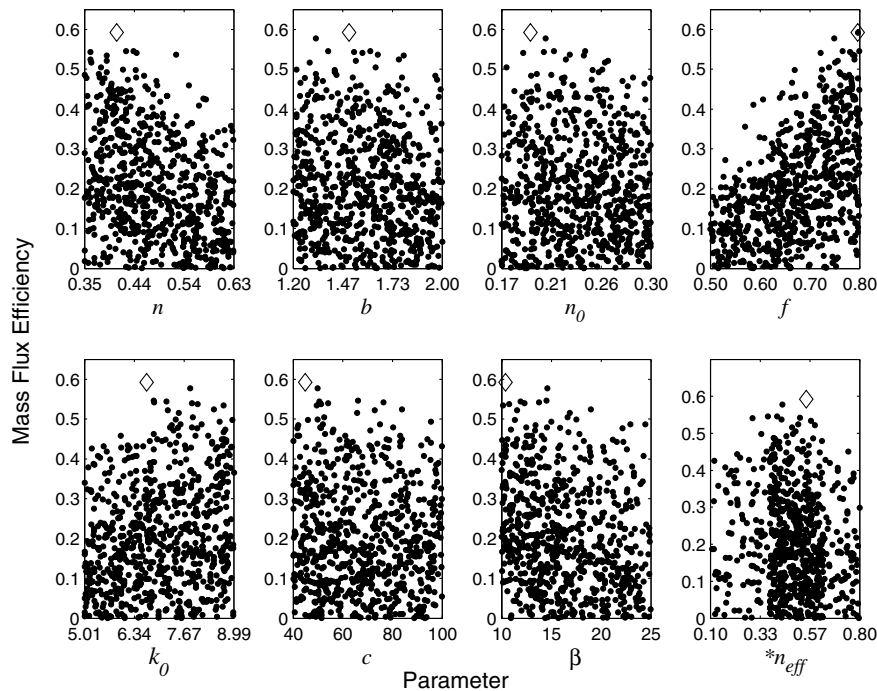

Fig. 5. A scattergram of 1000 Monte Carlo model simulations, where each point represents one model run with different randomly selected parameters within the range shown by the x-axes and its associated Nash–Sutcliffe efficiency [43] for mass flux. The large diamonds indicates the best parameter set for mass flux. Density changes in the $^*n_{eff}$ resulted from expanding the parameter range during the Monte Carlo simulation.

both parameter sets, suggesting that only half of the tracer was recovered during the field experiment possibly due to flow around the trench controlled by the bedrock topography.

4.3. Using the model to explore the transit time distribution

Using the best parameter sets from above, we simulated a constant rainfall rate of 0.2 mm h^{-1} for 416 days
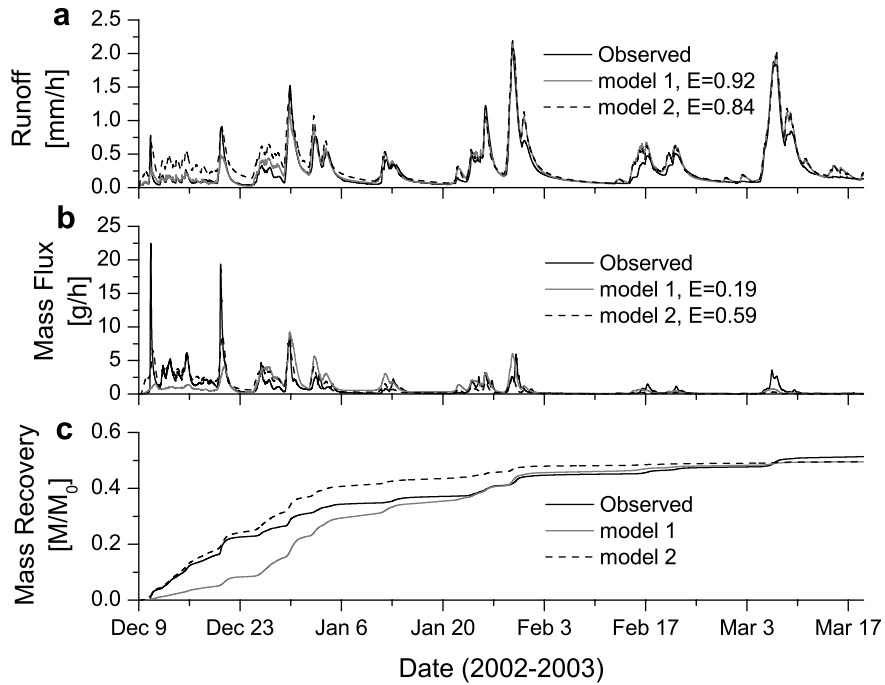
Fig. 6. Observed (solid black line) and simulated runoff (a), line-source tracer breakthrough as mass flux (b), and mass recovery (c). Gray lines indicate the best model fit to the observed runoff data (model 1) and dashed lines indicate the best model fit to the observed mass flux data (model 2). Nash–Sutcliffe efficiencies (*E*) [43] describing the goodness-of-fit are shown. The final mass recovery for both simulations was 50% and observed mass recovery was 53%.

(10,000 h) to calculate steady-state transit time distributions (TTDs). Once steady-state conditions were reached (83 days after rainfall initiation), we applied an instantaneous conservative tracer to the entire surface of the model domain. The resulting tracer breakthrough curves normalized according to Eq. (9) are shown in Fig. 7 for the parameter sets calibrated to runoff (model 1) and tracer mass flux (model 2). The mean transit times for the model simulations were 92 and 108 days for the models 1 and 2, respectively (Fig. 7). The TTDs describe the average transport
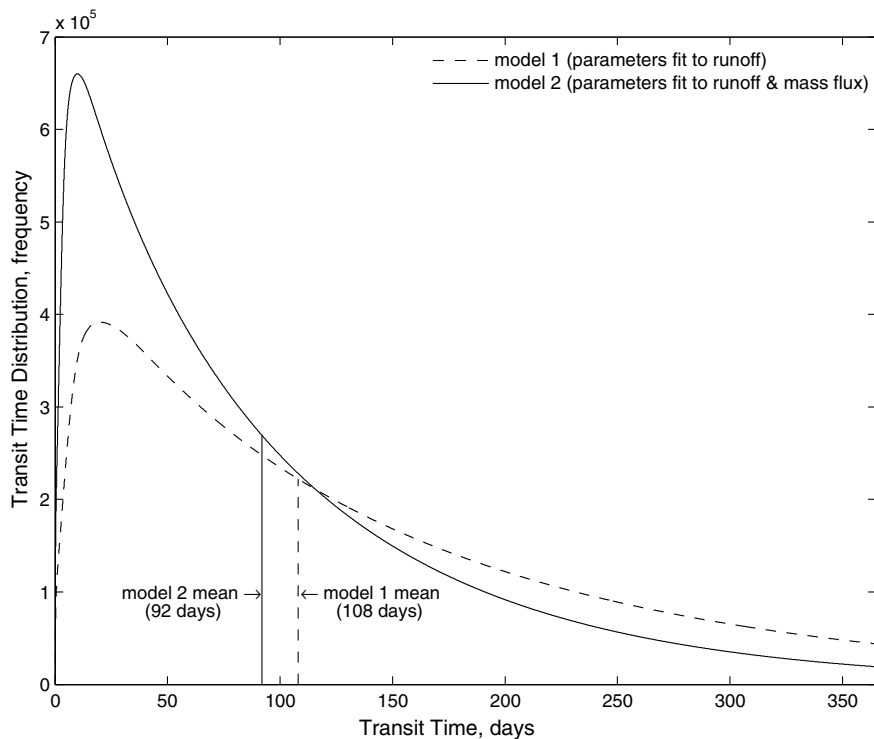

Fig. 7. Simulated transit time distributions for steady-state conditions derived from the models calibrated to runoff (model 1) and tracer mass flux (model 2).

behavior produced by the model with the two different parameter sets highlighting the need and value of a multi-criteria approach to calibration.

The simulated distribution (based on the model calibrated to tracer mass flux) is generally exponential (Fig. 8), but contains a distribution peak at 10 days. We tested the fit of common transit time distributions (e.g., the dispersion and gamma models), but they did not fit the simulated distribution better than the exponential distribution (or when the gamma distribution had a shape parameter equal to 1 (i.e., exponential) see [39]). The early time peak of the TTD indicates a lack of short flow pathways; nevertheless, it largely reflects the response of a well-mixed reservoir (i.e., an exponential TTD) where the outflow decreases monotonically due to mass loss from the hillslope and the lack of new tracer inputs.

The simulation of non-steady TTDs was carried out under a natural rainfall series and by applying separate conservative tracers to the model domain at different times of the year to examine the effect of antecedent wetness on the shape of the TTD. These results are shown in Fig. 9. Mean transit time varied between 54 and 69 days reflecting more rapid transport compared to the steady-state case. Cumulative forms of the TTDs are shown in Fig. 9b, since each individual TTD simulation is easier to distinguish in this form. The driest month, November, had the slowest mass recovery (55 d to recovery 50% mass) and wettest month had the most rapid mass recovery (23 d to recovery 50% mass) (Fig. 9). Recovery rates were most significantly

influenced by rainfall in the 30-day subsequent period after tracer application as opposed to 7 or 14 days after, or 7, 14, or 30 days before tracer application. The correlation between mass recovery rates for 25% and 50% recovery and the 30-day subsequent total rainfall were both 0.81, indicating that the hillslope more efficiently exported tracer when wet periods followed the tracer addition and thus yielded shorter TTDs.

The non-steady TTDs diverged from the simple exponential distribution that was fit to the mean transit time of all TTDs shown in Fig. 9. During the early time portion of the TTDs (i.e., transit times <100 d), most TTDs showed much more responsive behavior or weighting at early times in the breakthrough (the exception being the November TTD). Thus, the TTDs during wetter months recovered tracer much faster than the exponential distribution, which resulted in less mass recovered during later periods (i.e., transit times >150 d). This effect was largely controlled by the dry summer period (transit times between 150 and 260 d for most TTDs shown in Fig. 8), when subsurface flow velocities were significantly reduced. Interestingly, the general shape of TTDs reflects the exponential distribution perhaps deviating during early and late-time periods. The late-time period highlighted in the inset of Fig. 8a shows that tracer recovery for the March TTD resumed when the system wetted up after the summer drought period. This produced a slightly more linear tail on the logarithmic axes (non-exponential behavior) with 97% tracer recovery after 1 year.
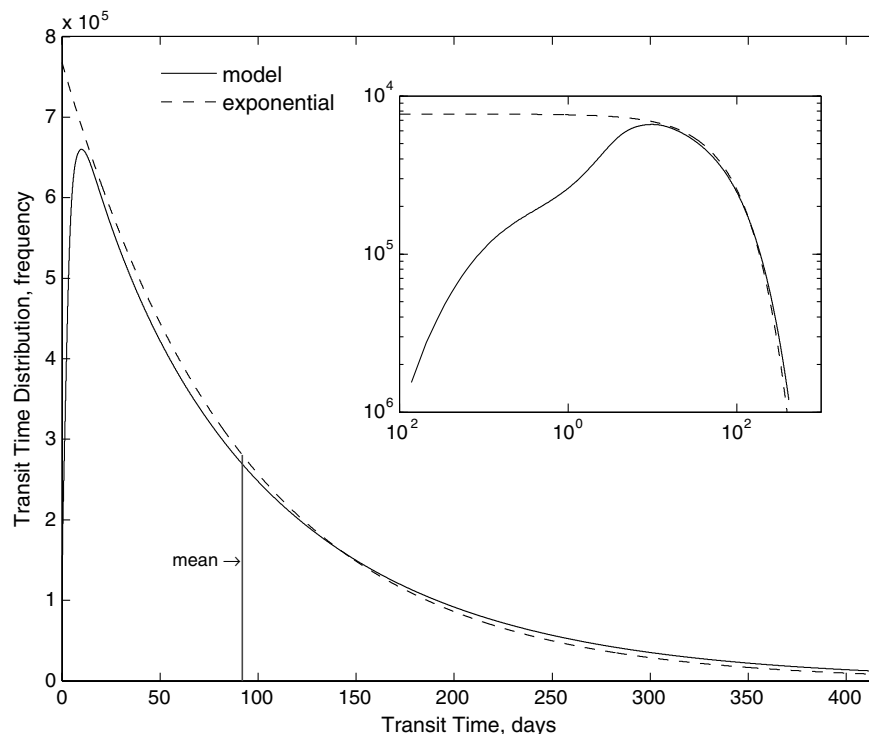

Fig. 8. Simulated transit time distribution (solid black line) for steady-state conditions (also shown as model 2 in Fig. 7) compared to an exponential distribution (dashed line). The vertical gray line shows the mean transit time for both distributions (92 days) and the inset plot shows the same distributions with logarithmic axes.
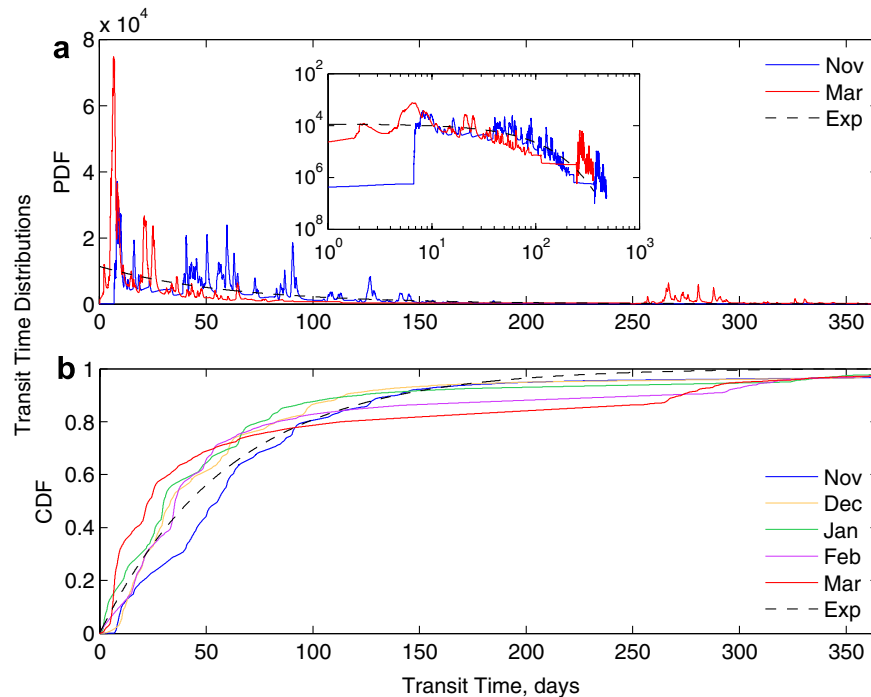
Fig. 9. Simulated transit time distributions for non-steady-state conditions compared to an exponential distribution (heavy solid black line). Select transit time distributions (November and March) are shown as probability density functions (PDFs) (a) and all transit time distributions are shown as cumulative density functions (CDFs) (b). The inset plot in (a) shows the PDFs on logarithmic axes.

5. Discussion

5.1. Model process representation

The two-part model calibration approach with runoff and the applied tracer experiment permitted the exploration of model complexity and process representation by our model. Runoff data alone did not contain enough information to represent the hydrological processes determined from field studies at this site, since many model parameters were not well-identified. The inclusion of the line-source tracer experiment and the additional calibration to mass flux, improved parameter identifiability, which provided further insight to the process controls on hillslope-scale water and solute flux. The measured K_{sat} values represented by the exponential depth function appeared to be too low for simulating tracer transport, especially deeper in the soil profile. This can be illustrated by examining the better performing values of f in Fig. 5 that approach the upper limit prescribed by the data indicating that better performance was achieved for higher K_{sat} values at depth. Also, effective porosity was quite important for simulating tracer mass flux, which suggests that an immobile soil fraction that controls the mixing volume is an important process to represent in the model structure. The bypass term did not appear to be as significant as we expected based on our field observations, which included dye staining experiments at a nearby site (e.g., [72]), and the observations presented in other published studies [26,28,47,65]. Optimized bypass parameters fit to both runoff and mass flux showed that smaller values (i.e., less bypass) produced better simulations. However, bypass was necessary to capture the general responsiveness of the tracer and water flux observed at the trench face.

Weiler and McDonnell [71] demonstrated that when drainable porosity was high (e.g., WS10 soils), modeled saturated zones were restricted in thickness, tracer mass exchange between the unsaturated and saturated zone was limited, and tracer movement was more affected by bedrock topography. In our study, the drainable porosity was important in modeling the rapid breakthrough of tracer, thin saturated zone development, and convergence of tracer along the bedrock surface towards trench face that resulted in similar modeled mass recovery compared to our field data. The sensitivity of tracer transport to the bedrock topography may have caused the observed recovery rates, which were constrained by the trench length and location relative to the bedrock topography.

5.2. Model inferred transit time distributions

The direct simulation of transit time distributions (TTDs) provided an experimental approach to estimating the TTD of a hillslope and insight to our model representation of flow pathways. The observed tracer breakthrough curves of Br^- and AGA suggested that extremely rapid contribution from upslope areas can occur within the timescale of a single storm event. Both the steady and non-steady-state TTD simulations indicated that peak tracer mass flux was delayed, although some tracer was trans-

ported from the hillslope within 1–2 days. This varied to some extent for the individual non-steady TTDs, since the tracer response was largely controlled by the timing of storm events. However, as illustrated by the steady-state TTD, when soil water deficits were no longer important, the main response occurred about 10 days after the modeled tracer injection with some contributions from short pathways that occurred within 1 day (Fig. 8).

Other studies have produced TTDs that are similarly shaped to the steady-state TTD found in this study. For example, Rodhe et al. [49] experimentally derived from a covered catchment study a TTD that was essentially exponential, but had a peak in the TTD at early time. Rodhe et al. [49] suggested the existence of a maximum peak in the TTD may not be significant and that the distribution approximates an exponential.

Simic and Destouni [54] derived the TTD produced in Rodhe et al. [49] theoretically using a stochastic-mechanistic model. Their theoretical model described non-uniform flow conditions resulting from groundwater recharge through the unsaturated zone, but also incorporated preferential flow, diffusional mass transfer between mobile and relatively immobile water, and random heterogeneity resulting from spatially variable transmissivity. While our steady-state model did not explicitly account for all of these processes (mainly because the water table was constant and no mass exchange occurred between the unsaturated and saturated zones), the non-steady TTDs that we simulated reflect many of theses processes such as time-variable recharge, preferential flow, and mass transfer between mobile/immobile domains (i.e., saturated/unsaturated zone) due to water table dynamics, suggesting that realistic hillslope TTDs are evidently more complex than the steady-state TTDs.

Under steady-state conditions, the unsaturated and saturated zones become effectively decoupled in our model, since water table fluctuations no longer rise and fall nor remobilize tracer in the unsaturated zone. A model that included interaction between the unsaturated and saturated zones was necessary to incorporate the dynamic behavior that was illustrated in the observed breakthrough curve and hence the true, unknown TTD. Even though the exponential distribution seemed to describe the predominant trend of the non-steady TTDs (Fig. 9), simplifying assumptions regarding the subsurface volume and mixing behavior in our model likely resulted in inaccurate late-time TTD behavior. For instance, the shapes of the TTD tails shown in Fig. 8 reflected a more power-law behavior (especially the March TTD) as did the observed breakthrough data. This was likely a model artifact of the well-mixed assumption in each zone (unsaturated and saturated) and model grid cell.

The simulated distributions found here were much younger than estimates based on observed stable isotope signatures (see [40]), which were on the order of 2 years old. There are two reasons for this discrepancy (1) the stable isotope estimates largely reflected baseflow conditions

(due to the runoff sampling routine described in McGuire et al. [40]), whereas this direct simulation approach incorporated the storm dynamics and (2) the mixing volume of our model did not include sources other than the regolith (i.e., no bedrock contribution). These observations reveal the need for future studies to incorporate bedrock contributions within catchment models that predict solute response and transit time investigations that include variable flow conditions.

5.3. On the value of integrating tracer experiments with hydrologic models

Since many catchment and hillslope scale applications require predictions concerning water quality, representing realistic transit time distributions and storage in hydrologic models is important. As demonstrated in this study by the high runoff efficiency achieved when only runoff was used to evaluate model performance, the best fitting model is not necessarily consistent with the internal process behavior as shown by the TTDs simulated using different parameter sets (Fig. 7). Applied tracer experiments offer an additional data source, which by nature, integrates flow heterogeneity into the tracer breakthrough. The breakthrough curve, like a hydrograph, reflects all of the physical process complexity into one signal and thus, provides an ideal source of information to help constrain parameterizations and reduce model uncertainty. Then, as shown in this study, a model calibrated to tracer data can be used to explore transit time distributions, which describe how potential contaminants and solutes are retained within a catchment or hillslope. Furthermore, the modeled transit time distribution can be drawn on to better understand the limitations of model structures and to independently assess the need to incorporate (or reject) additional process detail or heterogeneity as discussed in the previous section.

6. Conclusions

We argue that the combination of the tracer experiment, modeling exercise, and transit time simulation provides a more integrated approach to investigate runoff processes. These techniques helped to simplify observed process complexity and evaluate dominant physical processes used to structure the model. We presented a simple, spatially-explicit hydrologic model in order to identify the dominant processes necessary to explain both water and solute flux at the hillslope scale. This was accomplished by testing the model with a line-source tracer experiment, which improved parameter uncertainty, even though the overall model performance based on the fit to the runoff data decreased. The model was then used as an exploratory tool to infer potential transit time distributions that in turn assisted in the assessment of our model structure. The subsurface volume, the mixing assumption, and the water table dynamics were all found to be important controls on the distribution of transit times and potential areas of improvement within

our model framework. Further model improvements by including other data sources (e.g., groundwater levels) and developing more efficient computer code to run comprehensive uncertainty analyses are currently underway.

Acknowledgments

References

[1] Anderson MG, Burt TP. Process studies in hillslope hydrology. Chichester: Wiley; 1990.

[2] Bazemore DE, Eshleman KN, Hollenbeck KJ. The role of soil water in stormflow generation in a forested headwater catchment: synthesis of natural tracer and hydrometric evidence. J Hydrol 1994;162(1–2):47–75.

[3] Bear J. Dynamics of fluids in porous media. New York: American Elsevier Pub. Co.; 1972.

[4] Bergström S. Principles and confidence in hydrological modelling. Nord Hydrol 1991;22(2):123–36.

[5] Bergström S, Forsman A. Development of a conceptual deterministic rainfall-runoff model. Nord Hydrol 1973;4(3):147–70.

[6] Beven K. How far can we go in distributed hydrological modelling? Hydrol Earth Syst Sci 2001;5:1–12.

[7] Binley AM, Beven KJ, Calver A, Watts LG. Changing responses in hydrology: assessing the uncertainty in physically based model predictions. Water Resour Res 1991;27(6):1253–61.

[8] Blöschl G. Scaling in hydrology. Hydrol Processes 2001;15:709–11.

[9] Bonell M. Progress in the understanding of runoff generation dynamics in forests. J Hydrol 1993;150:217–75.

[10] Brammer D. Hillslope hydrology in a small forested catchment, Maimai, New Zealand. M.S. Thesis, State University of New York College of Environmental Science and Forestry, Syracuse; 1996.

[11] Brooks RH, Corey AT. Hydraulic properties of porous media. Colorado State University, Hydrology Paper 3; 1964.

[12] Buchter B, Hinz C, Leuenberger J. Tracer transport in a stony hillslope soil under forest. J Hydrol 1997;192:314–20.

[13] Burns DA, Hooper RP, McDonnell JJ, Freer JE, Kendall C, Beven K. Base cation concentrations in subsurface flow from a forested hillslope: the role of flushing frequency. Water Resour Res 1998;34(12):3535–44.

[14] Buttle JM, McDonald DJ. Coupled vertical and lateral preferential flow on a forested slope. Water Resour Res 2002;38(5). doi:10.1029/2001WR000773.

[15] Cirmo CP, McDonnell JJ. Linking the hydrologic and biochemical controls of nitrogen transport in near-stream zones of temperate-forested catchments: a review. J Hydrol 1997;199(1–2):88–120.

[16] Creed IF, Band LE. Exploring functional similarity in the export of ntirate-N from forested catchments: a mechanistic modeling approach. Water Resour Res 1998;34(11):3079–93.

[17] Doherty J, Johnston JM. Methodologies for calibration and predictive analysis of a watershed model. J Am Water Resour Assoc 2003;39(2):251–65.

[18] Dunne T. Field studies of hillsope flow processes. In: Kirkby MJ, editor. Hillslope hydrology. Chichester: Wiley; 1978. p. 227–93.

[19] Eriksson E. Compartment models and reservoir theory. Annu Rev Ecol Syst 1971;2:67–84.

[20] Franks SW, Gineste P, Beven KJ, Merot P. On constraining the predictions of a distributed model: the incorporation of fuzzy estimates of saturated areas into the calibration process. Water Resour Res 1998;34(4):787–97.

[21] Freer JE, McMillan H, McDonnell JJ, Beven KJ. Constraining dynamic TOPMODEL responses for imprecise water table information using fuzzy rule based performance measures. J Hydrol 2004;291(3-4):254–77.

[22] Güntner A, Uhlenbrook S, Seibert J, Leibundgut C. Multi-criterial validation of TOPMODEL in a mountainous catchment. Hydrol Processes 1999;13(11):1603–20.

[23] Hargreaves GH, Samani ZA. Reference crop evapotranspiration from temperature. Appl Eng Agric 1985;1(2):96–9.

[24] Harr RD. Water flux in soil and subsoil on a steep forested slope. J Hydrol 1977;33:37–58.

[25] Harr RD, Ranken DW. Movement of water through forested soils in steep topography. University of Washington, Coniferous Forest Biome Internal Report 117; 1972.

[26] Hornberger GM, Beven KJ, Germann PF. Inferences about solute transport in macroporous forest soils from time series models. Geoderma 1990;46:249–62.

[27] Jakeman AJ, Hornberger GM. How much complexity is warranted in a rainfall-runoff model? Water Resour Res 1993;29(8):2637–50.

[28] Jardine PM, Wilson GV, Luxmore RJ. Unsaturated solute transport through a forest soil during rain storm events. Geoderma 1990;46:103–18.

[29] Keim RF, Skaugset AE, Link TE, Iroumé A. A stochastic model of throughfall for extreme events. Hydrol Earth Syst Sci 2004;8(1):23–34.

[30] Klemeš V. Dilettantism in hydrology: transition or destiny. Water Resour Res 1986;22(9):177S–88S.

[31] Kuczera G, Mroczkowski M. Assessment of hydrologic parameter uncertainty and the worth of multiresponse data. Water Resour Res 1998;34:1481–9.

[32] Leaney FW, Smettem KRJ, Chittleborough DJ. Estimating the contribution of preferential flow to subsurface runoff from a hillslope using deuterium and chloride. J Hydrol 1993;147(1–4):83–103.

[33] Lindgren GA, Destouni G, Miller AV. Solute transport through the integrated groundwater-stream system of a catchment. Water Resour Res 2004;40:W03511. doi:10.1029/2003WR002765.

[34] Luxmoore RJ, Jardine PM, Wilson GV, Jones JR, Zelazny LW. Physical and chemical controls of preferred path flow through a forested hillslope. Geoderma 1990;46:139–54.

[35] Maloszewski P, Zuber A. Determining the turnover time of groundwater systems with the aid of environmental tracers. 1. Models and their applicability. J Hydrol 1982;57:207–31.

[36] Maloszewski P, Zuber A. Lumped parameter models for the interpretation of environmental tracer data. Manual on mathematical models in isotope hydrogeology, TECDOC-910. Vienna, Austria: International Atomic Energy Agency; 1996. p. 9–58.

[37] McDonnell JJ. A rationale for old water discharge through macropores in a steep, humid catchment. Water Resour Res 1990;26(11):2821–32.

[38] McDonnell JJ, Tanaka T. On the future of forest hydrology and biogeochemistry. Hydrol Processes 2001;15:2053–5.

[39] McGuire KJ, McDonnell JJ. A review and evaluation of catchment transit time modeling. J Hydrol [in press].

[40] McGuire KJ, McDonnell JJ, Weiler M, Kendall C, Welker JM, McGlynn BL, et al. The role of topography on catchment-scale water residence time. Water Resour Res 2005;41(5):W05002. doi:10.1029/2004WR003657.

[41] Montgomery DR, Dietrich WE, Torres R, Anderson SP, Heffner JT, Loague K. Hydrologic response of a steep, unchanneled valley to natural and applied rainfall. Water Resour Res 1997;33(1):91–109.

[42] Mroczkowski M, Raper GP, Kuczera G. The quest for more powerful validation of conceptual catchment models. Water Resour Res 1997;33(10):2325–35.

[43] Nash JE, Sutcliffe JV. River flow forecasting through conceptual models, I, A discussion of principles. J Hydrol 1970;10:282–90.

[44] Nyberg L, Rodhe A, Bishop K. Water transit times and flow path from two line injections of ^{3}H and ^{36}Cl in a microcatchment at Gardsjön, Sweden. Hydrol Processes 1999;13:1557–75.

[45] Nyström U. Transit time distributions of water in two forested catchments. In: Andersson F, Olsson B, editors. Lake Gårdsjön – an acid forest lake and its catchment; 1985. p. 97–100.

[46] Peters NE, Ratcliffe EB. Tracing hydrologic pathways using chloride at the Panola Mountain Research Watershed, Georgia, USA. Water Air Soil Pollut 1998;105(1-2):263–75.

[47] Radulovich R, Sollins P, Baveye P, Solórzano E. Bypass water flow through unsaturated microaggregated tropical soils. Soil Sci Soc Am J 1992;56:721–6.

[48] Ranken DW. Hydrologic properties of soil and subsoil on a steep, forested slope. MS Thesis, Oregon State University, Corvallis; 1974.

[49] Rodhe A, Nyberg L, Bishop K. Transit times for water in a small till catchment from a step shift in the oxygen 18 content of the water input. Water Resour Res 1996;32(12):3497–511.

[50] Rothacher J. Net precipitation under a Douglas-fir forest. Forest Science 1963;9(4):423–9.

[51] Seibert J, McDonnell JJ. On the dialog between experimentalist and modeler in catchment hydrology: use of soft data for multicriteria model calibration. Water Resour Res 2002;38(11):1241. doi:10.1029/2001WR000978.

[52] Seibert J, Rodhe A, Bishop K. Simulating interactions between saturated and unsaturated storage in a conceptual runoff model. Hydrol Processes 2003;17(2):379–90.

[53] Sidle RC, Hornbeck JW. Cumulative effects: a broader approach to water quality research. J Soil Water Conserv 1991;46(4):268–71.

[54] Simic E, Destouni G. Water and solute residence times in a catchment: stochastic-mechanistic model interpretation of ^{18}O transport. Water Resour Res 1999;35:2109–19.

[55] Sivapalan M. Process complexity at hillslope scale, process simplicity at the watershed scale: is there a connection? Hydrol Processes 2003;17(5):1037–41.

[56] Sivapalan M, Takeuchi K, Franks SW, Gupta VK, Karambiri H, Lakshmi V, et al. IAHS decade on predictions in ungauged basins (PUB), 2003–2012: shaping an exciting future for the hydrological sciences.. Hydrol Sci J 2003;48(6):857–80.

[57] Smart PL, Laidlaw IMS. An evaluation of some fluorescent dyes for water tracing. Water Resour Res 1977;13(1):15–33.

[58] Sollins P, McCorison FM. Nitrogen and carbon solution chemistry of an old growth coniferous forest watershed before and after cutting. Water Resour Res 1981;17:1409–18.

[59] Sollins P, Cromack KJ, McCorison FM, Waring RH, Harr RD. Changes in nitrogen cycling at an old-growth Douglas-fir site after disturbance. J Enivron Qual 1981;10:37–42.

[60] Stephens DB, Hsu K-C, Prieksat MA, Ankeny MD, Blandford N, Roth TL, et al. A comparison of estimated and calculated effective porosity. Hydrogeol J 1998;6(1):156–65.

[61] Stoddard JL, Jeffries DS, Lukewille A, Clair TA, Dillon DJ, Driscoll CT, et al. Regional trends in aquatic recovery from acidification in North America and Europe. Nature 1999;401(6753):575–8.

[62] Swanson FJ, James ME. Geology and geomorphology of the H. J. Andrews Experimental Forest, Western Cascades, Oregon, Pacific Northwest Forest and Range Experimental Station, PNW-188; 1975.

[63] Triska FJ, Sedell JR, Cromack K, Gregory SV, McCorison FM. Nitrogen budget for a small coniferous forest stream. Ecol Monogr 1984;54:119–40.

[64] Trudgill ST. Soil water dye tracing, with special reference to the use of Rhodamine WT, Lissamine FF and Amino G acid. Hydrol Processes 1987;1(2):149–70.

[65] Trudgill ST, Coles N. Application of simple soil-water flow models to the transfer of surface-applied solutes to streams. J Contam Hydrol 1988;3(2):367–80.

[66] Tsuboyama Y, Sidle RC, Noguchi S, Hosoda I. Flow and solute transport through the soil matrix and macropores of a hillslope segment. Water Resour Res 1994;30(4):879–90.

[67] Turner JV, Barnes CJ. Modeling of isotopes and hydrochemical responses in catchment hydrology. In: Kendall C, McDonnell JJ, editors. Isotope tracers in catchment hydrology. Amsterdam: Elsevier; 1998. p. 723–60.

[68] Uhlenbrook S, Leibundgut C. Process-oriented catchment modelling and multiple-response validation. Hydrol Processes 2002;16(2):423–40.

[69] USDA-NRCS. Soil taxonomy: a basic system of soil classification for making and interpreting soil surveys. 2d ed. Agricultural handbook 436. Washington (DC): United States Department of Agriculture, Natural Resources Conservation Service; 1999.

[70] Wagener T, McIntyre N, Lees MJ, Wheater HS, Gupta HV. Towards reduced uncertainty in conceptual rainfall-runoff modelling: dynamic identifiability analysis. Hydrol Processes 2003;17(2):455–76.

[71] Weiler M, McDonnell J. Virtual experiments: a new approach for improving process conceptualization in hillslope hydrology. J Hydrol 2004;285(1-4):3–18.

[72] Weiler M, Flühler H. Inferring flow types from dye patterns in macroporous soils. Geoderma 2004;120(1–2):137–53.

[73] Weiler M, McDonnell JJ. Testing nutrient flushing hypotheses at the hillslope scale: a virtual experiment approach. J Hydrol 2006;319(1–4):339–56.

[74] Weiler M, Uchida T, McDonnell J. Connectivity due to preferential flow controls water flow and solute transport at the hillslope scale. In: Proceedings of MODSIM 2003, Townsville, Australia; 2003.

[75] Wigmosta MS, Lettenmaier DP. A comparison of simplified methods for routing topographically driven subsurface flow. Water Resour Res 1999;35(1):255–64.

[76] Yoshinaga S, Ohnuki Y. Estimation of soil physical properties from a handy cone penetrometer test. Jpn Soc Erosion Contr Eng 1995;48(3):22–8.